Journal of Molecular Spectroscopy **201,** 267–279 (2000)
doi:10.1006/jmsp.2000.8099, available online at http://www.idealibrary.com on IDEAL®

Fourier Transform Emission Spectroscopy of the Low-Lying Electronic States of NbN

R. S. Ram and P. F. Bernath[1]

Department of Chemistry, University of Arizona, Tucson, Arizona 85721

Received December 8, 1999; in revised form February 24, 2000

The high-resolution spectrum of NbN has been investigated in emission in the 3000–15 000 cm^{-1} region using a Fourier transform spectrometer. The bands were excited in a microwave discharge through a mixture of $NbCl_5$ vapor, ~5 mTorr of N_2, and 3 Torr of He. Numerous bands observed in the near-infrared region have been classified into the following transitions: $f^1\Phi$–$c^1\Gamma$, $e^1\Pi$–$a^1\Delta$, $C^3\Pi_{0+}$–$A^3\Sigma_1^-$, $C^3\Pi_{0-}$–$A^3\Sigma_1^-$, $C^3\Pi_1$–$a^1\Delta$, $C^3\Pi_1$–$A^3\Sigma_0^-$, $d^1\Sigma^+$–$A^3\Sigma_0^-$, and $d^1\Sigma^+$–$b^1\Sigma^+$. These observations are consistent with the energy level diagram provided by laser excitation and emission spectroscopy [Y. Azuma, G. Huang, M. P. J. Lyne, A. J. Merer, and V. I. Srdanov, *J. Chem. Phys.* **100,** 4138–4155 (1993)]. The missing $d^1\Sigma^+$ state has been observed for the first time and its spectroscopic parameters are consistent with the theoretical predictions of S. R. Langhoff and W. Bauschlicher, Jr. [*J. Mol. Spectrosc.* **143,** 169–179 (1990)]. Rotational analysis of a number of bands has been obtained and improved spectroscopic parameters have been extracted for the low-lying electronic states. The observation of several vibrational bands with $v = 1$ has enabled us to determine the vibrational intervals and equilibrium bond lengths for the $A^3\Sigma_0^-$, $a^1\Delta$, $b^1\Sigma^+$, $d^1\Sigma^+$, and $C^3\Pi_1$ states.

INTRODUCTION

Over the last two decades considerable interest has developed in the spectroscopy of transition metal-containing molecules, partly due to the availability of many improved experimental and theoretical techniques. The inherent complexity of the electronic spectra of many transition metal oxides, nitrides, carbides, and halides has now been unraveled and successfully interpreted. The availability of high-quality *ab initio* calculations has proven to be very helpful in the analysis of these complex spectra. In part, the recent interest in the transition-metal-containing molecules can also be attributed to their importance in, for example, catalysis (*1, 2*) and astrophysics (*3*). Transition-metal atoms have relatively high abundances in many stars (*3*) and several transition-metal hydrides and oxides have also been detected (*3–8*). There is a possibility that transition-metal nitrides may also be found. So far nitride molecules have not been observed in stellar atmospheres, in part due to the lack of precise spectroscopic data required for a meaningful search in complex stellar spectra. In recent years, the electronic spectra of several transition-metal nitrides have been analyzed at high resolution and considerable progress has been made in theoretical studies (*9–12*), although much more work is needed. Only limited and fragmentary spectroscopic data are available for a number of transition-metal nitrides. For example, in the V B transition metal family, some high-resolution data are available for VN (*13, 14*) and NbN (*15–18*), but TaN (*19*) remains poorly characterized.

[1] Department of Chemistry, University of Waterloo, Waterloo, Ontario, Canada N2L 3G1.

The electronic spectra of NbN were first observed by Dunn and Rao in 1969 (*15*). The transition they saw was initially assigned as $A^3\Phi$–$X^3\Delta$ and the rotational analysis of the $^3\Phi_3$–$^3\Delta_2$ subband was reported. The rotational analysis of the other two subbands was difficult to achieve because of the presence of large nuclear hyperfine splittings at lower J values. The hyperfine structure of this transition was later analyzed by Féménias *et al.* (*16*) and more recently by Azuma *et al.* (*17*), and molecular constants including the hyperfine parameters have been determined. This transition was renamed as $B^3\Phi$–$X^3\Delta$ by Azuma *et al.* (*17*), who also recorded the laser excitation spectra of the $C^3\Pi$–$X^3\Delta$, $e^1\Pi$–$X^3\Delta_2$ and $f^1\Phi$–$a^1\Delta$ transitions and measured the spin–orbit intervals by observation of weak spin satellite branches (*17, 18*). The $^3\Delta_2$–$^3\Delta_1$ and $^3\Delta_3$–$^3\Delta_2$ intervals of 400.5 ± 0.1 and 490.5 ± 0.1 cm^{-1} were determined for the $X^3\Delta$ state of NbN. In addition, Azuma *et al.* (*18*) have observed a number of transitions between the low-lying singlet and triplet electronic states by recording the wavelength-resolved fluorescence following the selective laser excitation of different states. The term energy positions of the spin components of the $A^3\Sigma^-$, $B^3\Phi$, and $C^3\Pi$ triplet states as well as the positions of $a^1\Delta$, $b^1\Sigma^+$, $c^1\Gamma$, $e^1\Pi$, and $f^1\Phi$ singlet states were also determined in this work (*18*).

There have been several theoretical calculations that predict the dipole moments, dissociation energies, ionization potentials, and spectroscopic properties of the low-lying electronic state of NbN (*19–22*). The ionization potential of 7.175 eV was calculated by Bérces *et al.* (*20*) and the binding energy of 4.56 eV was calculated by Sellers (*21*) for the $X^3\Delta$ state of NbN. The permanent electric dipole moment of NbN was experimen-

0022-2852/00 $35.00

tally determined by Fletcher *et al.* (*22*) as 3.26(6) and 4.49(9) D for the $X^3\Delta_1$ and $B^3\Phi_2$ states, which compares well with the *ab initio* value of 3.65 *D* (*22*) obtained for the $X^3\Delta$ state. Their *ab initio* values of $r_e = 1.695$ Å and $\omega_e = 1010$ cm^{-1} also compare well with the experimental values of 1.663 Å and 1002.5 cm^{-1}, respectively. A very high-quality *ab initio* calculation has been performed by Langhoff and Bauschlicher (*23*) on the spectroscopic properties of the low-lying singlet and triplet electronic states of NbN. The ordering of states as well as the energy positions as determined experimentally by Azuma *et al.* (*18*) were found to be in excellent agreement with the predictions of Langhoff and Bauschlicher (*23*). The only exception was the $d^1\Sigma^+$ state, which was not observed directly by Azuma *et al.* (*18*) but was predicted by Langhoff and Bauschlicher (*23*) to be near 13 000 cm^{-1}.

In the present investigation we have recorded the emission spectrum of the red and near-infrared regions of NbN using a Fourier transform spectrometer. Numerous electronic transitions have been observed between the low-lying singlet and triplet states. The analysis of new bands is consistent with the energy level diagram provided for NbN by Azuma *et al.* (*18*). The missing $d^1\Sigma^+$ state has now been located from the observation of the $d^1\Sigma^+$–$A^3\Sigma_0^-$ and $d^1\Sigma^+$–$b^1\Sigma^+$ transitions. A rotational analysis has been performed for the numerous electronic transitions and improved spectroscopic constants have been evaluated.

EXPERIMENTAL DETAILS

The NbN emission bands were excited in an electrodeless microwave discharge through a flowing mixture of 3 Torr of He, about 5 mTorr of N_2, and a trace of $NbCl_5$ vapor. The discharge tube was made of quartz and had an outer diameter of 12 mm. Anhydrous $NbCl_5$ powder was placed in a small bulb which was continuously heated by a heating tape during the experiment. The partial pressure of $NbCl_5$ vapor in the discharge tube was adjusted to maintain a constant bluish–white color in the discharge. This experimental arrangement was chosen to simultaneously study the electronic spectra of NbCl and NbN in two experiments.

In the first experiment the discharge was made with 3 Torr of He and a trace of $NbCl_5$ vapor. This experiment was intended for the observation of NbCl spectra. Several NbCl bands, particularly those near 6704, 6799, and 6862 cm^{-1}, were observed with very weak intensity. In addition to NbCl, a number of NbO bands, with the most intense ones at 9306, 12 500, 12 571, 12 815, and 13 034 cm^{-1}, were also observed. The NbCl and NbO bands were distinguished by their line separation, with the branches in the NbCl bands having a smaller line spacing compared to those in NbO. The NbO bands were very recently observed by Launila *et al.* (*24*) and have been assigned to several doublet–doublet transitions.

In the second experiment ~5 mTorr of N_2 was added to the flow, keeping the other experimental parameters the same. In this case it was noticed that the NbO and NbCl bands again appeared along with new bands in the 8000–13 700 cm^{-1} region. These bands were later attributed to NbN using the results recently published by Azuma *et al.* (*18*). The NbN bands appeared strongly when the discharge had an intense blue–white color. The emission from the discharge tube was sent directly into the 8-mm entrance aperture of the 1-m Fourier transform spectrometer of the National Solar Observatory at Kitt Peak. The spectra in the 1800–15 000 cm^{-1} interval were recorded using liquid-nitrogen-cooled InSb detectors, a CaF_2 beam splitter, and RG695 filters. A total of six scans were co-added in about 63 min of integration at a resolution of 0.02 cm^{-1}.

The spectral line positions were determined using a data reduction program called PC-DECOMP developed by J. Brault. The peak positions were determined by fitting a Voigt lineshape function to each line. The strong N_2 lines observed in our spectra were used for calibration of the molecular lines of NbN. The strong N_2 lines recorded in a separate experiment with an Os hollow-cathode lamp operated with 10 mTorr of N_2 and 2.3 Torr of Ne were calibrated using the Ne line positions of Palmer and Engleman (*25*). This calibration was then transferred to the NbN spectrum using the N_2 lines as a transfer standard. The molecular lines of NbN have a typical width of 0.05 cm^{-1} and appear with a maximum signal-to-noise ratio of 12:1 so that the best line positions are expected to be accurate to about ± 0.002 cm^{-1}.

LOW-LYING ELECTRONIC STATES OF NbN

The ground state of NbN is now well established as a $^3\Delta$ state arising from the configuration, $4d\delta^1 5s\sigma^1$ (*17*, *18*, *23*). Until 1989 the only electronic transitions known for NbN were the $B^3\Phi$–$X^3\Delta$, $C^3\Pi$–$X^3\Delta$, and $C^3\Pi$–$A^3\Sigma^-$ transitions, where the $A^3\Sigma^-$, $B^3\Phi$, and $C^3\Pi$ states arise from $4d\delta^2$, $4d\delta^1 4d\pi^1$, and $4d\delta^1 4d\pi^1$ electron configurations, respectively. A very high-quality *ab initio* study of the spectroscopic properties of NbN was carried out by Langhoff and Bauschlicher (*23*), who calculated the properties of numerous low-lying singlet and triplet electronic states below 20 000 cm^{-1} as well as the quintet states below 30 000 cm^{-1} using the MRCI and MRCI + Q methods. Here MRCI denotes the multireference configuration interaction procedure based on SA-CASSCF (state-averaged complete-active-space self-consistent field) calculations and +Q refers to a Davidson-like correction. In the singlet manifold the ordering of the electronic states was predicted to be $a^1\Delta$ ($4d\delta^1 5s\sigma^1$), $b^1\Sigma^+$ ($5s\sigma^2$), $c^1\Gamma$ ($4d\delta^2$), $d^1\Sigma^+$ ($4d\delta^2$), and $e^1\Pi$ ($4d\delta^1 4d\pi^1$). In a recent publication, Azuma *et al.* (*18*) have reported the observation of a number transitions between the low-lying singlet and triplet electronic states which are consistent with the ordering of states predicted by Langhoff and Bauschlicher (*23*). The new transitions were observed by wavelength-resolved fluorescence with a small monochromator following selective laser excitation of various

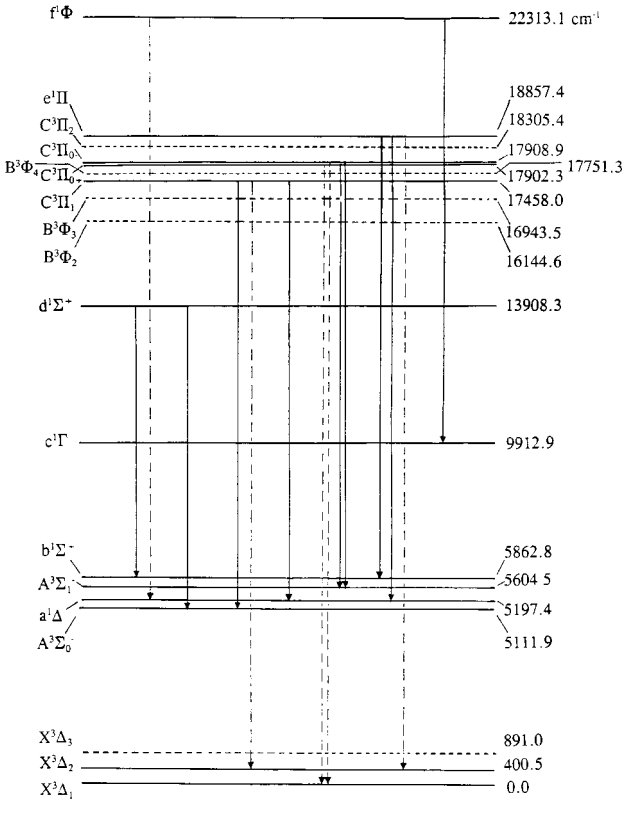

FIG. 1. A schematic energy level diagram of the observed electronic transitions of NbN. The positions of the $A^3\Sigma_0^-$, $a^1\Delta$, $b^1\Sigma^+$, $c^1\Gamma$, $d^1\Sigma^+$, $C^3\Pi_1$, and $f^1\Phi$ states have been drawn with the $X^3\Delta_2$–$X^3\Delta_1$ interval fixed to 400.5 cm^{-1} as determined by Azuma *et al.* (*18*) (see text for details). The positions of $X^3\Delta_3$, $B^3\Phi_2$, $B^3\Phi_3$, $B^3\Phi_4$, and $C^3\Pi_2$ states, marked by the broken lines, have been taken from the paper of Azuma *et al.* (*18*). The transitions marked with broken lines have been taken from the thesis of Huang (*26*).

excited states. The $d^1\Sigma^+$ state was not observed by Azuma *et al.* (*18*) and a high-lying $f^1\Phi$ ($4d\delta^1 4d\pi^1$) state was observed at 22 312 cm^{-1}. A summary of the low-lying electronic states of NbN has been provided in an energy level diagram in the paper by Azuma *et al.* (*18*). All of these states, except the $X^3\Delta$ state, have been observed in our present investigation of NbN using high-resolution Fourier transform emission spectroscopy. The missing $d^1\Sigma^+$ state has now been identified near 13 908 cm^{-1}. An updated energy level diagram of the low-lying electronic states has been provided in Fig. 1, where the observed T_{00} values of the low-lying states are also provided for reference.

OBSERVATIONS

A number of new NbN bands have been observed in the 8000–14 000 cm^{-1} region. The branches in different bands were sorted using a color Loomis–Wood program running on a PC computer. These bands have been found to involve numerous low-lying singlet states and spin components of the $C^3\Pi$ and $A^3\Sigma^-$ states. A schematic energy level diagram of observed low-lying electronic states is presented in Fig. 1. Although most of the states shown in this figure were observed previously by Azuma *et al.* (*18*), the infrared transitions marked in Fig. 1 have been observed at high resolution using a Fourier transform spectrometer. Also, the $d^1\Sigma^+$ state of NbN has been observed for the first time in our work.

(a) The $d^1\Sigma^+$–$b^1\Sigma^+$, $d^1\Sigma^+$–$A^3\Sigma_0^-$ Transitions

Two infrared transitions, which have 0–0 origins near 8045 and 8796 cm^{-1}, have a common upper state and are assigned as the $d^1\Sigma^+$–$b^1\Sigma^+$, $d^1\Sigma^+$–$A^3\Sigma_0^-$ transitions. These assignments locate the $d^1\Sigma^+$ state at 13 908 cm^{-1}. This state was not observed by Azuma *et al.* (*18*) but was predicted by Langhoff and Bauschlicher (*23*) at 14 908 and 12 878 cm^{-1} using the MRCI and MRCI + Q calculations, respectively. It was noted by Langhoff and Bauschlicher that the MRCI + Q calculations were in better agreement with the experimental values. The rotational structure of both of these transitions is slightly degraded toward higher wavenumbers because of the slightly smaller bond length of the $d^1\Sigma^+$ state compared with the bond lengths of the $b^1\Sigma^+$ and $A^3\Sigma_0^-$ states.

The spectrum of the $d^1\Sigma^+$–$b^1\Sigma^+$ transition near 8045 cm^{-1} is overlapped with a strong N_2 band near 8056 cm^{-1}. In spite of overlapping, the NbN rotational lines were easily distinguished because of relatively small separation between consecutive rotational lines in a branch. Our color Loomis–Wood program was also very helpful in identifying the lines in the overlapped regions. This band consists of one R and one P branch and lines have been identified up to $R(37)$ and $P(42)$. The 0–0 band is followed by relatively weaker 1–1 and 2–2 bands with origins near 8069 and 8093 cm^{-1}. The rotational structure of all three bands has been analyzed.

The 0–0 band of the $d^1\Sigma^+$–$A^3\Sigma_0^-$ transition has its origin near 8796 cm^{-1}. This region of the spectrum is relatively free from N_2 overlapping. The band also consists of single R and P branches, as expected. A part of the spectrum of this transition is provided in Fig. 2, where P-branch lines of the 0–0 band have been marked up to the bandhead. We have identified the

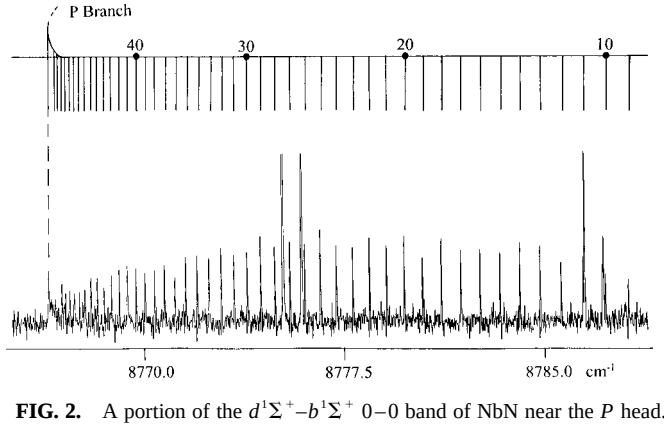

FIG. 2. A portion of the $d^1\Sigma^+$–$b^1\Sigma^+$ 0–0 band of NbN near the P head.

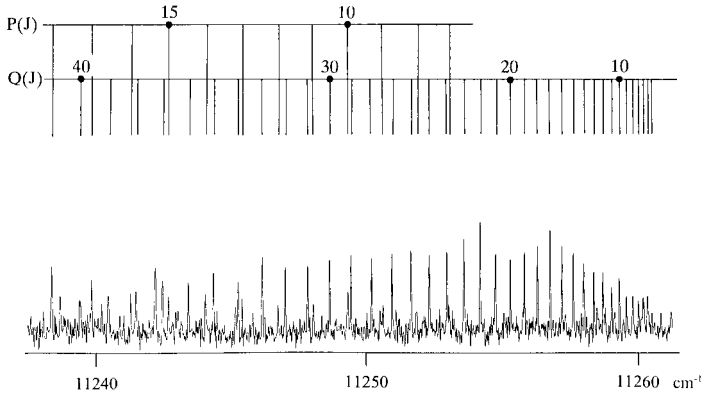

FIG. 3. A portion of the $C^3\Pi_1$–$a^1\Delta$ 0–0 band of NbN near the Q head.

lines up to $R(53)$ and $P(54)$ in this band. The 1–1 and 2–2 bands of this transition have also been observed near 8821 and 8846 cm^{-1} with relatively weak intensity and a rotational analysis of 0–0, 1–1, and 2–2 bands has been obtained.

(b) The $C^3\Pi_1$–$a^1\Delta$ and $C^3\Pi_1$–$A^3\Sigma_0^-$ Transitions

Two bands observed near 12 261 and 12 346 cm^{-1} have an excited state in common. These bands were assigned as the 0–0 bands of the $C^3\Pi_1$–$a^1\Delta$ and $C^3\Pi_1$–$A^3\Sigma_0^-$ transitions. Both of these transitions consist of P, Q, and R branches with the Q branch being the most intense.

The $C^3\Pi_1$–$a^1\Delta$ transition at 12 261 cm^{-1} has a relatively open structure and the rotational lines in the three branches are clearly resolved starting from close to the origin. The higher J lines with $J \geq 35$ slowly broaden due to the onset of small Λ-doubling in the $C^3\Pi_1$ state but the split lines could not be measured because of their very weak intensity. Lines up to $R(34)$, $P(34)$, and $Q(39)$ were observed in the 0–0 band. A part of the spectrum of this transition near the Q head is presented in Fig. 3, where some P and Q lines have been marked. The 1–1 band of this transition has an R head at 12 195.7 cm^{-1} and all the three branches were identified in this band. The rotational analysis of both 0–0 and 1–1 bands was obtained.

In the 0–0 band of the $C^3\Pi_1$–$A^3\Sigma_0^-$ transition near 12 346 cm^{-1}, the lines of the Q branch are not resolved and most of the Q lines pile up in a 2 cm^{-1} interval to the lower wavenumber side of the origin. This is a result of the near equality of the rotational constants in the upper and lower states. In this case the R and P branches have a open structure. The 1–1 band of this transition appears with a Q head near 12 309.5 cm^{-1} and the Q branch is partly resolved at higher J values. A compressed portion of the spectrum of NbN in the $C^3\Pi$–$A^3\Sigma^-$ region is provided in Fig. 4, where the Q heads of the 0–0 and 1–1 bands have been marked. The 0–0 Q heads of the $C^3\Pi_0$–$A^3\Sigma_1^-$ and $f^1\Phi$–$c^1\Gamma$ transitions, presented in the following sections, have also been marked in this figure. The R and P lines of the 0–0 and 1–1 bands were picked out with the help of our Loomis–Wood program and were rotationally analyzed. The line positions of the 0–0 and 1–1 bands of the $C^3\Pi_1$–$X^3\Delta_2$ transition (*26*) with the same excited state were also included in the final fit. To constrain the $\Delta G(\frac{1}{2})$ vibrational interval of the $X^3\Delta_2$ spin component, the difference between the Q-branch lines of the 1–0 and 1–1 bands of the $B^3\Phi_3$–$X^3\Delta_2$ transition (*26*) were also included in the fit. This was necessary to determine the vibrational intervals of the excited states.

(c) The $C^3\Pi_{0+}$–$A^3\Sigma_1^-$ and $C^3\Pi_{0-}$–$A^3\Sigma_1^-$ Transition

Two bands with Q heads near 12 297.7 and 12 304.3 cm^{-1}, which appear with moderate intensity, have been found to have their lower states in common. These two bands have been identified as the 0–0 bands of the $C^3\Pi_{0+}$–$A^3\Sigma_1^-$ and $C^3\Pi_{0-}$–$A^3\Sigma_1^-$ transitions. The Q branch of the $C^3\Pi_{0+}$–$A^3\Sigma_1^-$ 0–0 band is shaded toward the higher wavenumbers and is partly resolved while the Q branch of the $C^3\Pi_{0-}$–$A^3\Sigma_1^-$ 0–0 band is unresolved with slight shading toward lower wavenumbers

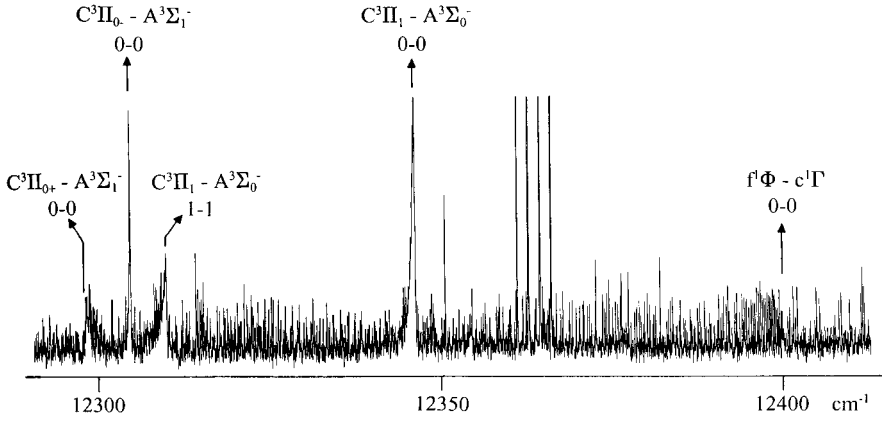

FIG. 4. A compressed portion of the spectrum of NbN showing the Q heads of the $C^3\Pi_{0+}$–$A^3\Sigma_1^-$, $C^3\Pi_{0-}$–$A^3\Sigma_1^-$, $C^3\Pi_1$–$A^3\Sigma_0^-$, and $f^1\Phi$–$c^1\Gamma$ electronic transitions of NbN.

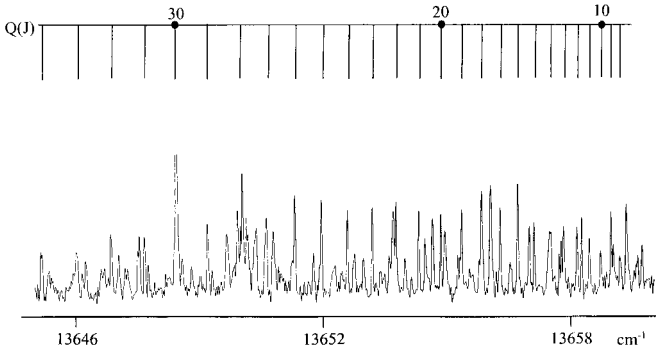

FIG. 5. A portion of the $e^1\Pi$–$a^1\Delta$ 0–0 band of NbN near the Q head.

(Fig. 4). Although the R and P branches of these bands are weaker in intensity and are not distinguishable at first sight, our Loomis–Wood program was very helpful in identifying the lines. Also the known combination differences for the $C^3\Pi_{0-}$ state based on the previous work of Azuma *et al.* (*18*) were very useful in making definite assignments. The 1–1 bands of these two transitions could not be identified due to their very weak intensity. Rotational analysis of both 0–0 bands has been carried out. The line positions of the $C^3\Pi_{0+}$–$X^3\Delta_1$ and $C^3\Pi_{0-}$–$X^3\Delta_1$ 0–0 transitions (*26*) were also included in the final fit.

(d) The $e^1\Pi$–$a^1\Delta$ and $e^1\Pi$–$b^1\Sigma^+$ Transitions

Two bands observed with Q heads near 13 660 and 12 994.5 cm^{-1} have been identified as the 0–0 bands of the $e^1\Pi$–$a^1\Delta$ and $e^1\Pi$–$b^1\Sigma^+$ transitions. The 1–1 bands of these two transitions were not identified. The $e^1\Pi$–$a^1\Delta$ 0–0 band at 13 660 cm^{-1} consists of three branches P, Q, and R, with the Q branch being the most intense. A part of the 0–0 band of this transition is presented in Fig. 5, where some lines in the Q branch have been marked. The high J lines of this band slowly broaden and split in two components near $J = 35$ because of the small Λ-doubling in the $e^1\Pi$ state. The high J lines after the Λ-doubling is resolved were very weak and could not be reliably measured. We have identified lines up to $R(37)$, $P(42)$, and $Q(46)$ in this band.

The $e^1\Pi$–$b^1\Sigma^+$ 0–0 band at 12 994.6 cm^{-1} is much weaker in intensity than the $e^1\Pi$–$a^1\Delta$ band and is overlapped with N_2 and NbO lines present in the same region. The Q lines of this band could be readily identified from the predictions based on constants of the $e^1\Pi$ and $b^1\Sigma^+$ states. The R and P lines of this band are too weak to be measured. This band was not included in the final fit.

(e) The $f^1\Phi$–$c^1\Gamma$ Transition

A band observed with a Q head at 12 400 cm^{-1} has been identified as the 0–0 band of $f^1\Phi$–$c^1\Gamma$ transition. This band consists of P, Q, and R branches with the Q branch being the most intense. The rotational structure of this band is partly overlapped with the lines of the $C^3\Pi_1$–$A^3\Sigma_0^-$ 0–0 band on the lower wavenumber side and a NbO band on the higher wavenumber side but could be positively identified with the help of our Loomis–Wood program. The previously reported data for the $f^1\Phi$–$a^1\Delta$ transition (*26*) were also helpful in the assignment of this band. A part of the Q branch of this band near the band origin is presented in Fig. 6. No Λ-doubling has been observed as expected for a $^1\Phi$–$^1\Gamma$ transition and we have identified the lines up to $R(48)$, $P(44)$, and $Q(55)$. The lines of the 0–0 $f^1\Phi$–$a^1\Delta$ transition (*26*) were also included in the final fit.

ANALYSIS

The observed line positions of bands of the different electronic transitions are provided in Table 1. The molecular constants for different states were determined by fitting the observed line positions to the following customary energy level expressions:

(for $^1\Sigma^+$, $^3\Sigma_0^-$, $^1\Delta$, $^1\Phi$, and $^1\Gamma$ states)

$$F_v(J) = T_v + B_vJ(J+1) - D_v[J(J+1)]^2, \qquad [1]$$

(for $^1\Pi$, $^3\Sigma_1^-$, and $^3\Pi_1$ states)

$$F_v(J) = T_v + B_vJ(J+1) - D_v[J(J+1)]^2 \pm 1/2\{qJ(J+1) + q_D[J(J+1)]^2\}. \qquad [2]$$

Two fits were obtained for the determination of final spectroscopic constants. In the first fit the lines of the $C^3\Pi_{0+}$–$A^3\Sigma_1^-$ and $C^3\Pi_{0-}$–$A^3\Sigma_1^-$ transitions were combined with the line positions of the $C^3\Pi_{0+}$–$X^3\Delta_1$, $C^3\Pi_{0-}$–$X^3\Delta_1$ transitions previously observed by laser excitation spectroscopy (*18*, *26*). In the second fit lines from the $d^1\Sigma^+$–$A^3\Sigma_0^-$, $d^1\Sigma^+$–$b^1\Sigma^+$, $C^3\Pi_1$–$A^3\Sigma_0^-$, $C^3\Pi_1$–$a^1\Delta$, $e^1\Pi$–$a^1\Delta$, and $f^1\Phi$–$c^1\Gamma$ transitions were fit simultaneously. The rotational lines of the $C^3\Pi_1$–$X^3\Delta_2$, $e^1\Pi$–$X^3\Delta_2$, and $f^1\Phi$–$a^1\Delta$ transitions from the previous laser excitation work (*26*) were also included in this fit so that all of the new bands are connected together and referenced to $v = 0$ of the $X^3\Delta_2$ spin component. The badly blended lines

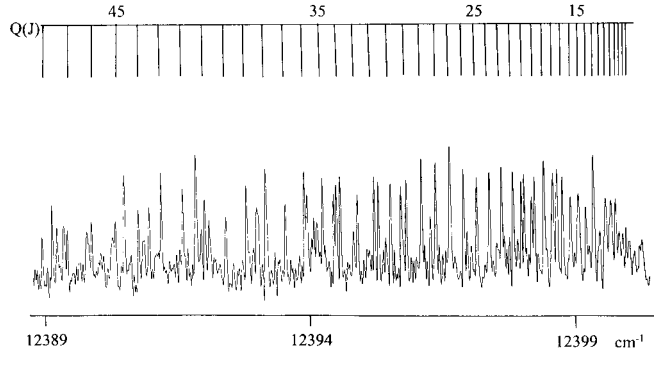

FIG. 6. A portion of the $f^1\Phi$–$c^1\Gamma$ 0–0 band of NbN near the Q head.

TABLE 1

Observed Line Positions (in cm^{-1}) of the Near-Infrared Transitions of NbN

J	R(J)	O-C	P(J)	O-C	R(J)	O-C	P(J)	O-C	R(J)	O-C	P(J)	O-C
	$d^1\Sigma^+ - b^1\Sigma^+$, 0-0				$d^1\Sigma^+ - b^1\Sigma^+$, 1-1				$d^1\Sigma^+ - b^1\Sigma^+$, 2-2			
1	8047.491	6										
2	8048.507	-5										
3	8049.544	-3	8042.494	3								
4	8050.595	3	8041.515	-5								
5	8051.647	2	8040.554	-3			8064.064	-1			8087.538	0
6	8052.709	1	8039.607	3	8076.151	-9	8063.140	19			8086.599	-2
7	8053.780	0	8038.659	-2	8077.223	-7	8062.187	0	8100.644	-2	8085.674	-2
8	8054.860	-1	8037.724	-2	8078.308	-3	8061.255	-7	8101.728	2	8084.765	4
9	8055.950	-1	8036.802	1	8079.397	-4	8060.348	1	8102.816	0	8083.858	2
10	8057.055	5	8035.888	3			8059.445	3	8103.926	9		
11	8058.160	2	8034.977	-2	8081.618	7			8105.025	-3	8082.077	-1
12	8059.274	-1	8034.081	-1	8082.731	2	8057.661	-0	8106.146	-2		
13	8060.403	1	8033.193	-0	8083.858	0	8056.789	3	8107.280	1	8080.338	-4
14	8061.540	3	8032.315	0	8084.995	-2	8055.921	0				
15	8062.679	-2	8031.446	-1			8055.068	3	8109.565	-7	8078.648	0
16	8063.833	-1	8030.586	-1	8087.302	0	8054.220	0	8110.735	1	8077.819	2
17	8065.004	6	8029.736	-1	8088.470	1	8053.383	-2	8111.913	7	8076.994	-2
18	8066.169	-0	8028.898	3	8089.651	4	8052.559	0	8113.091	3		
19	8067.348	-2	8028.063	-1			8051.741	-3	8114.277	-4	8075.390	4
20	8068.540	1	8027.240	-3	8092.033	3	8050.939	-0	8115.487	4	8074.620	23
21	8069.739	1	8026.430	0	8093.237	2	8050.143	-0	8116.697	1	8073.816	-3
22	8070.947	1	8025.626	-1	8094.451	0	8049.360	1	8117.920	2	8073.049	-3
23	8072.163	0	8024.831	-3	8095.670	-6	8048.580	-4	8119.152	1	8072.310	15
24	8073.388	-1	8024.050	-0	8096.925	14	8047.817	-2			8071.546	-3
25	8074.620	-4	8023.276	-0	8098.161	5	8047.066	1			8070.814	1
26	8075.864	-3	8022.513	1	8099.412	2	8046.321	0			8070.088	-1
27	8077.123	2	8021.757	-0	8100.675	1	8045.585	-2			8069.377	2
28	8078.383	-1	8021.012	-0	8101.947	-1	8044.862	-1			8068.674	1
29	8079.651	-3	8020.282	5	8103.226	-5	8044.149	-1			8067.984	3
30			8019.547	-5	8104.528	4	8043.457	9			8067.293	-6
31			8018.839	3			8042.757	1			8066.626	-3
32	8083.514	-10	8018.132	2	8107.141	1	8042.072	-3			8065.969	-1
33	8084.832	0	8017.436	1			8041.400	-3			8065.327	5
34			8016.750	1	8109.799	5	8040.740	-2			8064.685	-0
35	8087.480	5	8016.076	4	8111.139	3					8064.064	6
36	8088.809	-1	8015.405	-2							8063.440	-4
37	8090.166	11	8014.759	8			8038.817	-7			8062.837	-3
38			8014.104	-1			8038.202	-3			8062.264	18
39			8013.481	11			8037.597	-1			8061.666	2
40			8012.846	3			8036.995	-6			8061.081	-13
41			8012.225	-3			8036.411	-4				
42			8011.621	-2			8035.835	-6				
43												
44							8034.725	1				
45							8034.184	3				
46							8033.655	6				
47							8033.142	12				
	$d^1\Sigma^+ - A^3\Sigma_0^-$, 0-0				$d^1\Sigma^+ - A^3\Sigma_0^-$, 1-1				$d^1\Sigma^+ - A^3\Sigma_0^-$, 2-2			
1	8798.444	5										
2	8799.480	-1										
3	8800.535	-3	8793.477	-5								
4	8801.608	-3	8792.540	0	8826.008	-4	8816.995	9			8842.070	15
5	8802.703	1	8791.609	-5	8827.094	-4	8816.062	-4			8841.139	-2
6	8803.807	-1	8790.704	-0	8828.208	7	8815.162	-1	8853.217	-2	8840.251	6
7	8804.940	10	8789.808	-4			8814.279	2	8854.334	-1	8839.374	9
8	8806.072	3	8788.933	-2	8830.455	-1	8813.411	4	8855.463	-5	8838.503	0
9	8807.225	0	8788.076	1	8831.613	4	8812.566	12	8856.628	11	8837.657	-0
10	8808.397	0	8787.231	-1	8832.772	-5	8811.720	1	8857.787	4	8836.819	-9

Note. O-C are observed minus calculated line positions in units of 10^{-3} cm^{-1}.

TABLE 1—*Continued*

J	R(J)	O-C	P(J)	O-C	R(J)	O-C	P(J)	O-C	R(J)	O-C	P(J)	O-C
11	8809.585	1	8786.405	-0	8833.962	-1	8810.896	-4	8858.967	1	8836.015	-2
12	8810.787	-1	8785.595	0	8835.178	13	8810.097	-1	8860.165	-1	8835.236	13
13	8812.011	2	8784.802	1	8836.382	-2	8809.310	-2	8861.392	9	8834.452	7
14	8813.247	2	8784.027	3	8837.617	-2	8808.541	-2	8862.615	-1	8833.689	4
15	8814.499	-0	8783.266	3	8838.866	-4	8807.795	4	8863.866	0	8832.937	-4
16	8815.769	1	8782.520	1	8840.140	2	8807.058	2	8865.130	-2	8832.210	-4
17	8817.052	-2	8781.795	3	8841.424	2	8806.336	-2	8866.407	-8	8831.489	-16
18	8818.354	-1	8781.083	2	8842.727	4	8805.633	-3	8867.715	-0	8830.803	-10
19	8819.673	-0	8780.389	2	8844.042	1	8804.940	-11	8869.033	1	8830.138	1
20	8821.006	-1	8779.710	-0	8845.373	-1	8804.289	5	8870.360	-5	8829.482	3
21	8822.357	0	8779.049	0	8846.728	4	8803.636	3	8871.714	-0	8828.842	3
22	8823.724	0	8778.404	-1	8848.094	3	8802.996	-3	8873.080	-1	8828.208	-6
23	8825.107	0	8777.777	0	8849.478	4	8802.382	0	8874.463	-1	8827.609	1
24	8826.504	-1	8777.166	-0	8850.874	1	8801.782	-0			8827.014	-4
25	8827.918	-1	8776.575	3	8852.285	-4	8801.199	1			8826.449	4
26	8829.349	-2	8775.994	-1			8800.629	-4			8825.893	3
27	8830.803	5	8775.435	1	8855.169	-0	8800.085	2			8825.362	11
28	8832.260	-1	8774.890	1	8856.628	-6	8799.552	1			8824.839	9
29	8833.742	2	8774.363	0	8858.115	-0	8799.035	0			8824.330	4
30	8835.236	0	8773.851	-1	8859.603	-10	8798.536	-0			8823.842	3
31	8836.745	-2	8773.359	1	8861.122	-4	8798.057	2			8823.364	-6
32	8838.274	-0	8772.881	-0	8862.660	5	8797.593	3			8822.915	-2
33	8839.820	2	8772.423	2	8864.197	-5	8797.142	-1			8822.484	3
34	8841.376	-1	8771.979	1	8865.768	4	8796.715	2			8822.057	-6
35	8842.953	-0	8771.551	0	8867.340	-3	8796.306	8			8821.651	-11
36	8844.541	-4	8771.137	-3	8868.939	1	8795.902	-1			8821.288	10
37	8846.156	4	8770.747	-0	8870.549	-0	8795.530	7			8820.914	3
38	8847.776	1	8770.372	1	8872.176	0	8795.154	-7			8820.560	-1
39	8849.413	-1	8770.011	-0	8873.822	2	8794.813	-3			8820.222	-8
40	8851.068	-1	8769.668	-1			8794.486	-1			8819.915	1
41	8852.740	-1	8769.344	0			8794.181	5			8819.620	3
42	8854.425	-3	8769.035	-0			8793.880	-2			8819.332	-3
43	8856.138	6	8768.743	1			8793.596	-8				
44	8857.850	-1	8768.465	-2			8793.339	-6				
45	8859.585	0	8768.209	-0			8793.098	-4				
46	8861.338	1	8767.970	2			8792.878	1				
47	8863.098	-5	8767.743	-1			8792.676	8				
48	8864.882	-4	8767.535	-1			8792.469	-7				
49	8866.678	-5	8767.346	0			8792.312	9				
50	8868.496	-2	8767.176	4			8792.148	3				
51	8870.314	-13	8767.016	1								
52	8872.176	3	8766.877	2								
53	8874.039	4	8766.740	-13								
54			8766.634	-14								

J	R(J)	O-C	Q(J)	O-C	P(J)	O-C	R(J)	O-C	Q(J)	O-C	P(J)	O-C
			$C^3\Pi_{0+} - A^3\Sigma_1^-$, 0-0						$C^3\Pi_{0-} - A^3\Sigma_1^-$, 0-0			
6							12311.351	-7				
7							12312.373	6				
8							12313.374	-3	Unresolved			
9							12314.380	-11	Q-head at			
10							12315.396	-10	12304.35			
11					12286.794	-1	12316.423	-0	cm^{-1}			
12	12310.616	4			12285.803	6	12317.442	0				
13	12311.593	-4			12284.801	3	12318.469	6			12291.654	-6
14	12312.578	-3			12283.797	-1	12319.499	12			12290.710	10
15	12313.561	-3			12282.799	-0					12289.735	-7
16	12314.552	5			12281.799	0	12321.537	-3			12288.786	0
17	12315.528	-1			12280.796	-2	12322.572	3			12287.829	-4
18	12316.514	4			12279.805	8	12323.595	-5			12286.888	6
19	12317.488	-2	12298.145	-2	12278.801	5	12324.631	-3			12285.931	-2

TABLE 1—*Continued*

J	R(J)	O-C	Q(J)	O-C	P(J)	O-C	R(J)	O-C	Q(J)	O-C	P(J)	O-C
20	12318.469	-0	12298.193	5	12277.796	2	12325.665	-4			12284.989	2
21	12319.445	-2	12298.234	3	12276.795	2	12326.705	-0			12284.041	-2
22	12320.426	1	12298.278	2	12275.794	4	12327.749	6			12283.098	-2
23	12321.398	-4	12298.326	3	12274.784	-3	12328.781	-3			12282.159	-2
24	12322.373	-5	12298.374	3	12273.793	9	12329.823	-2			12281.220	-3
25	12323.347	-5	12298.422	1	12272.777	-3	12330.878	10			12280.294	6
26	12324.324	-1	12298.476	3	12271.780	4	12331.917	3			12279.358	3
27	12325.293	-5	12298.525	-2	12270.779	8	12332.969	9			12278.423	-2
28	12326.269	-0	12298.578	-3	12269.765	-1	12333.999	-9			12277.499	3
29	12327.236	-4	12298.639	0	12268.759	-2	12335.057	-1			12276.563	-6
30	12328.210	1	12298.694	-3	12267.757	2	12336.111	3			12275.653	8
31	12329.169	-8	12298.762	4	12266.739	-10	12337.156	-5			12274.717	-5
32	12330.144	1	12298.819	0	12265.740	-2	12338.203	-11			12273.797	-5
33	12331.110	1	12298.882	-0	12264.740	5	12339.269	0			12272.880	-4
34	12332.072	-1	12298.948	2	12263.728	1	12340.326	1			12271.961	-6
35	12333.039	2	12299.007	-5	12262.714	-5	12341.385	4			12271.051	-2
36	12333.999	1	12299.084	5	12261.710	-0	12342.437	-3			12270.144	4
37	12334.961	3	12299.153	5	12260.700	-2	12343.498	-0				
38			12299.216	-2							12268.318	-3
39	12336.872	-3	12299.294	6	12258.682	0	12345.625	5			12267.416	2
40	12337.832	2	12299.364	3	12257.676	5	12346.687	5			12266.508	-1
41	12338.786	1	12299.434	1	12256.663	4	12347.743	-1			12265.613	8
42	12339.726	-12	12299.501	-6	12255.660	12	12348.813	6			12264.695	-8
43	12340.691	2	12299.578	-5			12349.872	1			12263.806	2
44	12341.639	0	12299.660	1			12350.930	-6			12262.911	6
45	12342.580	-7	12299.740	4			12352.000	-1			12262.002	-6
46			12299.810	-4			12353.070	4			12261.121	8
47			12299.899	7			12354.138	6			12260.214	-5
48			12299.980	8							12259.326	-1
49											12258.431	-5
50			12300.124	-9								
51			12300.213	-0								
52			12300.295	-1								
53			12300.380	2								
			$C^3\Pi_1 - A^3\Sigma_0^-$, 0-0						$C^3\Pi_1 - A^3\Sigma_0^-$, 1-1			
9											12300.599	8
10											12299.587	-1
11	12357.899	0	Unresolved		12335.121	0					12298.578	-4
12	12358.871	-5	Q-head at		12334.113	-6	12322.170	-8			12297.582	7
13	12359.848	-4	12346.06		12333.121	5	12323.140	4			12296.567	0
14	12360.825	-2	cm^{-1}		12332.121	9					12295.544	-12
15	12361.798	-2			12331.110	4	12325.048	3			12294.544	1
16	12362.768	-4			12330.096	-4	12325.990	-7			12293.530	1
17	12363.741	-2			12329.092	-2	12326.954	8			12292.501	-12
18	12364.715	2			12328.087	2	12327.889	-4			12291.499	4
19	12365.683	3			12327.080	3	12328.845	7			12290.471	-4
20	12366.651	5			12326.066	-1	12329.777	-3			12289.448	-5
21	12367.613	1			12325.048	-8	12330.730	9			12288.428	-3
22	12368.577	2			12324.040	-4	12331.663	5			12287.399	-6
23	12369.536	-1			12323.031	-0	12332.589	-5			12286.385	7
24	12370.495	-3			12322.017	-1	12333.522	-6			12285.357	8
25	12371.454	-3					12334.452	-6	12308.909	11	12284.319	0
26	12372.406	-9			12319.989	1	12335.396	9	12308.856	10	12283.274	-12
27	12373.373	3			12318.971	-0	12336.302	-10	12308.807	15	12282.248	-4
28	12374.326	2			12317.951	-3	12337.230	-6	12308.748	13	12281.220	5
29	12375.277	1			12316.937	2	12338.146	-11	12308.683	6		
30	12376.216	-11			12315.916	0	12339.074	-1	12308.622	5		
31	12377.173	-2			12314.896	2	12339.981	-9	12308.564	10		
32	12378.124	1			12313.884	12	12340.891	-12	12308.496	7		
33	12379.070	2			12312.850	0	12341.803	-11	12308.432	10		
34	12380.014	3			12311.824	-1	12342.709	-13	12308.351	-1		

TABLE 1—*Continued*

J	R(J)	O-C	Q(J)	O-C	P(J)	O-C	R(J)	O-C	Q(J)	O-C	P(J)	O-C
35	12380.954	3			12310.802	1			12308.289	9		
36	12381.883	-8			12309.776	1			12308.210	4		
37	12382.826	-2			12308.748	2			12308.134	5		
38	12383.771	8			12307.712	-6			12308.052	1		
39	12384.701	5			12306.686	-2			12307.973	3		
40	12385.624	-2			12305.662	5			12307.884	-2		
41	12386.555	-0			12304.629	4						
42	12387.483	2			12303.586	-6						
43					12302.555	-2						
44	12389.329	2			12301.522	1						
45	12390.251	6			12300.471	-12						
46	12391.171	9			12299.434	-10						
47	12392.076	-1										
48	12392.982	-6										
49	12393.881	-16										
50	12394.804	2										
			$C^3\Pi_1 - a^1\Delta$, 0-0						$C^3\Pi_1 - a^1\Delta$, 1-1			
6			12260.051	-10								
7			12259.877	-3	12252.935	-12	12184.469	-12				
8	12268.586	-3	12259.675	-0	12251.741	-10	12185.248	-2				
9	12269.337	-11	12259.447	4	12250.528	-1	12185.991	-2	12176.161	11	12167.279	-13
10	12270.080	-0	12259.190	4	12249.281	-1	12186.706	-1			12166.031	-8
11	12270.779	-8	12258.907	4	12248.012	2	12187.393	-2	12175.588	2	12164.755	-4
12	12271.464	-4	12258.596	2	12246.712	1			12175.262	-1	12163.466	13
13	12272.124	1	12258.262	2	12245.392	5	12188.700	10	12174.909	-4	12162.133	13
14			12257.902	2	12244.037	0	12189.291	-5	12174.538	2	12160.758	-2
15	12273.352	-3	12257.516	2	12242.667	6	12189.880	5	12174.138	5	12159.364	-9
16	12273.943	11	12257.105	3	12241.263	3			12173.706	4	12157.964	5
17	12274.490	8	12256.663	-1	12239.829	-4	12190.956	4	12173.245	1	12156.517	-2
18	12275.007	-1	12256.201	0	12238.379	-2			12172.761	1	12155.053	1
19	12275.508	2	12255.714	3	12236.899	-4	12191.926	6	12172.249	0	12153.557	-1
20	12275.991	12	12255.195	-0	12235.399	-1	12192.369	5	12171.710	0	12152.029	-8
21	12276.427	2	12254.656	2	12233.867	-3	12192.788	8	12171.145	1	12150.489	-1
22	12276.847	1	12254.090	3	12232.318	3			12170.553	2	12148.914	-1
23	12277.232	-8	12253.494	1	12230.732	-2	12193.529	-1	12169.931	0	12147.315	1
24	12277.606	-2	12252.875	1	12229.123	-5	12193.866	3	12169.285	2	12145.688	3
25	12277.953	4	12252.231	2	12227.496	1	12194.172	2	12168.606	-4	12144.030	-0
26	12278.264	-0	12251.557	-0	12225.840	2	12194.452	3	12167.900	-8	12142.337	-11
27	12278.555	2	12250.860	-0	12224.152	-2	12194.697	-2	12167.181	1	12140.627	-12
28	12278.801	-14	12250.135	-1	12222.445	0	12194.925	1	12166.421	-3	12138.898	-5
29	12279.048	-2	12249.387	-0	12220.709	0	12195.109	-10	12165.634	-7	12137.138	-3
30	12279.265	5	12248.610	-2	12218.956	8	12195.299	11	12164.825	-5	12135.351	-0
31	12279.439	-3	12247.807	-3	12217.161	0	12195.425	-4	12163.991	-1	12133.533	-1
32	12279.584	-14	12246.984	2	12215.345	-4	12195.543	1	12163.129	2	12131.693	2
33	12279.714	-14	12246.136	9	12213.505	-5	12195.627	0	12162.226	-9	12129.828	8
34	12279.805	-26	12245.251	4	12211.650	4	12195.691	7	12161.321	7	12127.906	-17
35			12244.339	-1					12160.365	-3	12125.987	-10
36			12243.409	3					12159.401	8		
37			12242.447	0					12158.394	4		
38			12241.463	2					12157.354	-6		
39			12240.446	-2					12156.307	5		
J	Ree(J)	O-C	Pee(J)	O-C	Rff(J)	O-C	Pff(J)	O-C	Qfe(J)	O-C	Qef(J)	O-C
						$e^1\Pi - a^1\Delta$, 0-0						
5									13659.704	5	13659.704	5
6	13666.499	11			13666.499	10			13659.559	9	13659.559	10
7	13667.306	1			13667.306	1						
8	13668.104	7	13651.245	-0	13668.104	6	13651.245	-1	13659.170	-6	13659.170	-5
9	13668.855	-8	13650.042	12	13668.855	-9	13650.042	11	13658.954	2	13658.954	3
10	13669.599	-6	13648.786	-4	13669.599	-7	13648.786	-5	13658.702	-1	13658.702	-0
11	13670.313	-9	13647.535	9	13670.313	-11	13647.535	8	13658.432	2	13658.432	4
12	13671.006	-7	13646.231	-5	13671.006	-9	13646.231	-6	13658.132	2	13658.132	3

TABLE 1—*Continued*

J	Ree(J)	O-C	Pee(J)	O-C	Rff(J)	O-C	Pff(J)	O-C	Qfe(J)	O-C	Qef(J)	O-C
13	13671.671	-8	13644.917	-4	13671.671	-10	13644.917	-6	13657.805	-2	13657.805	-1
14	13672.304	-16	13643.586	4	13672.304	-18	13643.586	3	13657.457	-0	13657.457	1
15	13672.937	1	13642.217	-0	13672.937	-1	13642.217	-2	13657.080	-4	13657.080	-2
16	13673.529	3	13640.828	-0	13673.529	1	13640.828	-2	13656.686	1	13656.686	3
17	13674.100	8			13674.100	7			13656.260	0	13656.260	2
18	13674.627	-4	13637.977	1	13674.627	-5	13637.977	-0	13655.811	1	13655.811	3
19	13675.149	3	13636.511	-0	13675.149	2	13636.511	-2	13655.334	-1	13655.334	0
20	13675.636	2	13635.020	-2	13675.636	1	13635.020	-4	13654.836	1	13654.836	2
21	13676.093	-5	13633.509	0	13676.093	-4	13633.509	-0	13654.309	-0	13654.309	-0
22	13676.532	-4	13631.972	2	13676.532	-2	13631.972	1	13653.757	-1	13653.757	-2
23	13676.941	-6	13630.405	-1	13676.941	-4	13630.405	-1	13653.182	-0	13653.182	-1
24	13677.334	-0			13677.334	3			13652.582	3	13652.582	0
25	13677.690	-5	13627.208	5	13677.690	-0	13627.208	7	13651.953	1	13651.953	-3
26	13678.022	-8	13625.560	-4	13678.022	-2	13625.560	-0	13651.305	6	13651.305	2
27	13678.338	-1	13623.895	-5	13678.338	7	13623.895	-1	13650.619	-1	13650.619	-7
28	13678.618	-4	13622.205	-5	13678.618	6	13622.205	1	13649.919	4	13649.919	-4
29	13678.874	-6			13678.874	6			13649.188	3	13649.188	-7
30	13679.106	-5	13618.759	4	13679.106	10	13618.759	14	13648.447	18	13648.447	6
31	13679.337	20	13616.978	-12	13679.289	-9	13616.978	0	13647.655	9	13647.655	-6
32	13679.508	12	13615.192	-8	13679.469	-6	13615.192	7	13646.839	2	13646.845	-11
33	13679.671	22	13613.377	-7	13679.620	-3	13613.377	11	13646.012	9	13646.043	18
34	13679.786	11			13679.745	-1			13645.146	4	13645.178	11
35	13679.891	15			13679.837	-5	13609.650	-1	13644.263	8	13644.289	4
36	13679.955	5	13607.790	6	13679.891	-20	13607.745	-9	13643.336	-6	13643.382	7
37	13680.013	16			13679.955	2			13642.400	-1	13642.459	19
38			13603.926	4			13603.884	-0				
39			13601.955	2			13601.902	-7	13640.440	-2	13640.496	4
40			13599.961	2			13599.900	-8			13639.479	0
41			13597.948	10			13597.869	-12	13638.369	-6	13638.443	4
42			13595.897	6			13595.821	-7	13637.298	-3	13637.367	-6
43									13636.189	-12	13636.281	0
44											13635.156	-5
45											13634.010	-6
46											13632.840	-4

J	R(J)	O-C	Q(J)	O-C	P(J)	O-C	J	R(J)	O-C	Q(J)	O-C	P(J)	O-C
						$f^1\Phi - c^1\Gamma$							
9			12399.746	-7	12390.854	8	33	12428.455	-1	12394.884	-1	12362.302	7
10			12399.663	3	12389.766	2	34			12394.560	0		
11			12399.552	-6	12388.673	2	35	12429.762	2	12394.223	-1	12359.676	6
12			12399.450	5	12387.566	-5	36	12430.396	0	12393.879	-0	12358.345	2
13	12413.173	-4	12399.325	1	12386.450	-10	37	12431.024	3	12393.520	-4	12357.004	-1
14	12414.040	5	12399.188	-6	12385.347	6	38	12431.640	4	12393.156	-1	12355.663	4
15	12414.891	8	12399.049	-4	12384.214	1	39	12432.239	-0	12392.781	-0	12354.297	-5
16	12415.722	1	12398.901	-2	12383.072	-3	40	12432.832	0	12392.399	5	12352.934	-2
17	12416.555	4	12398.746	1	12381.930	4	41	12433.415	1	12391.997	-1	12351.555	-4
18	12417.370	0	12398.568	-8	12380.772	2	42	12433.977	-8	12391.582	-8	12350.168	-5
19	12418.175	-4	12398.395	-2	12379.607	3	43	12434.553	10	12391.173	1	12348.775	-2
20	12418.973	-5	12398.213	3	12378.426	-3	44			12390.741	-2	12347.374	4
21	12419.767	-1	12398.012	-1	12377.234	-11	45	12435.634	4	12390.311	7		
22			12397.803	-3	12376.048	-3	46	12436.155	-1	12389.856	2		
23	12421.321	4	12397.589	0	12374.849	1	47	12436.666	-4	12389.397	4		
24	12422.080	4	12397.364	1	12373.632	-3	48	12437.170	-3	12388.918	-3		
25	12422.826	-0	12397.128	1	12372.406	-7	49			12388.436	-2		
26	12423.572	6	12396.879	-2	12371.182	1	50			12387.936	-9		
27	12424.290	-5	12396.625	-0	12369.943	2	51			12387.444	4		
28	12425.015	-0	12396.358	-2	12368.692	2	52			12386.929	5		
29	12425.724	-0	12396.090	5	12367.430	-1	53			12386.393	-3		
30			12395.802	2	12366.156	-4	54			12385.859	1		
31	12427.105	-6	12395.506	1	12364.885	3	55			12385.308	-1		
32	12427.789	-1	12395.198	-2	12363.592	-1							

TABLE 2
Spectroscopic Constants (in cm^{-1}) for Low-Lying Electronic States of NbN

	v	T_v	B_v	$10^7 \times D_v$	$10^3 \times q_v$	$10^8 \times q_{Dv}$
$X^3\Delta_1$	0	0.0	0.5001157(65)	4.528(27)	--	--
$X^3\Delta_2$	0	400.5 [a]	0.5017295(48)	4.792(22)	--	--
	1	1434.5755(14) [a]	0.4991097(63)	4.606(34)	--	--
$A^3\Sigma_0^-$	0	5111.8916(12) [a]	0.4958108(47)	4.711(19)	--	--
	1	6128.4693(26) [a]	0.4931750(76)	4.716(41)	--	--
	2	b	0.490593(27)	5.08(29)	--	--
$A^3\Sigma_1^-$	0	5604.53298(84)	0.4960528(65)	4.623(28)	-1.3243(17)	2.64(11)
$a^1\Delta$	0	5197.37374(93) [a]	0.5081547(51)	4.650(24)	--	--
	1	6260.6461(19) [a]	0.5056439(73)	4.556(42)	--	--
$b^1\Sigma^+$	0	5862.8389(15) [a]	0.4994432(52)	5.003(23)	--	--
	1	6880.3653(29) [a]	0.4966393(82)	5.056(43)	--	--
	2	b+753.5050(13)	0.493884(27)	5.39(29)	--	--
$c^1\Gamma$	0	9912.8939(19) [a]	0.4995986(63)	4.804(30)	--	--
$d^1\Sigma^+$	0	13908.2989(13) [a]	0.5040215(47)	4.721(19)	--	--
	1	14949.3000(28) [a]	0.5015045(82)	4.734(46)	--	--
	2	b+8845.87816(92)	0.499041(28)	5.18(31)	--	--
$C^3\Pi_1$	0	17457.97432(54) [a]	0.4953024(45)	5.073(18)	--	--
	1	18438.0057(15) [a]	0.4922086(64)	4.959(36)	--	--
$C^3\Pi_{0-}$	0	17908.89147(45)	0.4965409(65)	5.017(27)	--	--
$C^3\Pi_{0+}$	0	17902.28158(43)	0.4964593(64)	5.016(27)	--	--
$e^1\Pi$	0	18857.4454(11) [a]	0.4957215(54)	5.509(27)	-0.0145(25)	3.00(21)
$f^1\Phi$	0	22313.0661(18) [a]	0.4949508(61)	5.382(29)	--	--

Note. All term values marked with "a" were fitted with respect to the $v = 0$ vibrational level of the $X^3\Delta_2$ spin component which was held fixed to the value of 400.5 cm^{-1} obtained by Azuma *et al.* (*18*), while "b" refers to the undetermined term value for the $v = 2$ vibrational level of the $A^3\Sigma_0^-$ state.

were given reduced weights and overlapped lines were excluded in order to improve the standard deviation of the fit. The first fit is connected to $v = 0$ of the lowest energy $X^3\Delta_1$ spin component while the second fit is connected to $v = 0$ of the $X^3\Delta_2$ spin component. Because we have no direct connection between the energy levels in our two separate fits, we have chosen to fix the $v = 0$ $X^3\Delta_2$–$X^3\Delta_1$ interval to exactly 400.5 cm^{-1}. The molecular constants obtained for the different electronic states are provided in Table 2.

DISCUSSION

The energy level diagram of the low-lying electronic states obtained by Azuma *et al.* (*18*) was very helpful in assigning the new transitions observed in the present work. The position of the new transitions, except those involving the $d^1\Sigma^+$ state, were readily calculated by taking the difference between the term values of the different electronic states. The $d^1\Sigma^+$ state was not observed by Azuma *et al.* (*18*) and was not marked in their energy level diagram. The observation of two transitions, $d^1\Sigma^+$–$A^3\Sigma_0^-$ and $d^1\Sigma^+$–$b^1\Sigma^+$, with a common excited state provided a straightforward assignment of the rotational lines. The $d^1\Sigma^+$ state has been located at 13 908 cm^{-1} at the energy scale adopted by Azuma *et al.* (*18*). This compares with the calculated position of 12 878 cm^{-1} from MRCI + Q calculation of Langhoff and Bauschlicher (*23*). A revised energy level diagram of the observed low-lying singlet and triplet electronic states of NbN is provided

TABLE 3
Equilibrium Constants (in cm^{-1}) $A^3\Sigma_0^-$, $a^1\Delta$, $b^1\Sigma^+$, $d^1\Sigma^+$, and $C^3\Pi_1$ States of NbN

Const.[a]	$A^3\Sigma_0^-$	$a^1\Delta$	$b^1\Sigma^+$	$d^1\Sigma^+$	$C^3\Pi_1$
$\Delta G(1/2)$	1016.5777(29)	1063.2724(21)	1017.5264(33)	1041.0011(31)	980.0314(16)
B_e	0.497124(13)	0.5094101(68)	0.500840(12)	0.505275(12)	0.4968493(60)
α_e	0.002628(13)	0.0025108(89)	0.002796(13)	0.002509(13)	0.0030938(78)
r_e(Å)	1.669320(22)	1.649066(11)	1.663115(20)	1.655800(19)	1.669781(10)

[a]Numbers in parentheses are one standard deviation in the last digits.

in Fig. 1. The term energies of different electronic states are on the same scale as given by Azuma *et al.* (*18*).

The electronic transitions observed in our work involve singlet–singlet or singlet–triplet transitions and hyperfine splitting or broadening has not been detected. As has been noted previously, the $B^3\Phi$–$X^3\Delta$ and $C^3\Pi$–$X^3\Delta$ transitions show strong hyperfine effects which result mainly from the large Nb hyperfine splitting in the $X^3\Delta$ state (*17, 18*). The molecular constants obtained from the final fit are presented in Table 2. Inspection of this table indicates that the $^3\Sigma_0^-$ and $^3\Sigma_1^-$ spin components of the $A^3\Sigma^-$ state are about 492 cm^{-1} apart, which is not normal for a Hund's case (b) $^3\Sigma^-$ state. This indicates that the $A^3\Sigma^-$ state is better described by Hund's case (c) coupling. This case (c) behavior is a result of the interaction of the $A^3\Sigma_0^-$ spin component with the higher lying $b^1\Sigma^+$ and $d^1\Sigma^+$ states. As discussed in detail by Azuma *et al.* (*18*), the $b^1\Sigma^+$ $(5s\sigma^2)$ state is mixed with the $d^1\Sigma^+(4d\delta^2)$ state by electrostatic perturbation. Because of this interaction the $b^1\Sigma^+$ state acquires considerable $d^1\Sigma^+$ character and thus perturbs the $A^3\Sigma_0^-$ spin component more strongly because it lies much closer to the $A^3\Sigma_0^-$ state.

During the rotational and hyperfine analysis of the $C^3\Pi$–$X^3\Delta$ transition, Azuma *et al.* (*17, 18*) found evidence of strong second-order spin–orbit interaction between the $C^3\Pi$ and $e^1\Pi$ states, both arising from the same valence electron configuration, $4d\delta^1 4d\pi^1$. Because of this interaction, the $C^3\Pi_1$ spin component is pushed down 650 cm^{-1} from the expected position by the $e^1\Pi$ state. The $e^1\Pi$–$X^3\Delta_2$ intercombination transition was observed strongly because of these interactions. We have also observed the $C^3\Pi_1$–$a^1\Delta$ intercombination transition in addition to the $C^3\Pi_1$–$A^3\Sigma_0^-$ and $C^3\Pi_0$–$A^3\Sigma_0^-$ transitions.

The molecular constants of the $A^3\Sigma_0^-$, $a^1\Delta$, $b^1\Sigma^+$, $d^1\Sigma^+$, and $C^3\Pi_1$ states (Table 2) have been used to evaluate the equilibrium rotational constants for these states, which are provided in Table 3. Even though the 2–2 bands were observed in the $d^1\Sigma^+$–$b^1\Sigma^+$ and $d^1\Sigma^+$–$A^3\Sigma_0^-$ transitions, the $v = 2$ vibrational levels of the $b^1\Sigma^+$ and $d^1\Sigma^+$ states remain floating because there is no connection with the known vibrational levels of the $C^3\Pi_1$ state. Equilibrium vibrational constants for the $A^3\Sigma_0^-$, $b^1\Sigma^+$, and $d^1\Sigma^+$ states could, therefore, not be determined in spite of the observation of $v = 0$, 1, and 2 vibrational levels. The equilibrium rotational constants provide the equilibrium bond lengths of 1.669320(22), 1.649066(11), 1.663115(20), 1.655800(19), and 1.669781(10) Å for the $A^3\Sigma_0^-$, $a^1\Delta$, $b^1\Sigma^+$, $d^1\Sigma^+$, and $C^3\Pi_1$ states, respectively.

CONCLUSION

The emission spectrum of NbN has been investigated at high resolution in the 3000–15 000 cm^{-1} region using a Fourier transform spectrometer. The bands observed in the 8000–14 000 cm^{-1} region have been assigned to a number of transitions involving both singlet and triplet electronic states. Rotational analysis of these transitions has been carried out and improved spectroscopic constants have been obtained for most of the low-lying states. In this work we have located the missing $d^1\Sigma^+$ state, which was predicted by Langhoff and Bauschlicher (*23*), but was not observed experimentally in previous investigations (*18, 26*). The observation of the 0–0 and 1–1 bands in a number of transitions, in conjunction with the previously reported wavenumbers for several transitions, have enabled us to determine the $\Delta G(\frac{1}{2})$ vibrational intervals as well as equilibrium bond lengths for $A^3\Sigma_0^-$, $a^1\Delta$, $b^1\Sigma^+$, $d^1\Sigma^+$, and $C^3\Pi_1$ states of NbN. Our observations are in excellent agreement with the *ab initio* predictions of Langhoff and Bauschlicher (*23*) and the previous work of Azuma *et al.* (*18*).

ACKNOWLEDGMENTS

We thank M. Dulick of the National Solar Observatory for assistance in obtaining the spectra. The National Solar Observatory is operated by the Association of Universities for Research in Astronomy, Inc. under contract with the National Science Foundation. The research described here was supported by funding from the NASA laboratory astrophysics program. Support was also provided by the Petroleum Research Fund administered by the American Chemical Society and the Natural Sciences and Engineering Research Council of Canada. We thank A. Merer for providing a copy of the Ph.D. thesis of G. Huang.

REFERENCES

1. M. Grunze *in* "The Chemical Physics of Solid Surfaces and Heterogeneous Catalysis" (D. A. King and D. P. Woodruff, Eds.), Vol. 4, p. 143, Elsevier, New York, 1982.
2. F. A. Cotton, G. Wilkinson, C. A. Murillo, and M. Bochman, "Advanced Inorganic Chemistry," 6th ed., Wiley, New York, 1999.
3. C. Jascheck and M. Jascheck, "The Behavior of Chemical Elements in Stars," Cambridge University Press, Cambridge, UK, 1995.

4. D. L. Lambert and R. E. S. Clegg, *Mon. Not. R. Astron. Soc.* **191,** 367–389 (1980).
5. R. Yerle, *Astron. Astrophys.* **73,** 346–351 (1979).
6. B. Lindgren and G. Olofsson, *Astron. Astrophys.* **84,** 300–303 (1980).
7. O. Engvold, H. Wöhl, and J. W. Brault, *Astron. Astrophys. Suppl. Ser.* **42,** 209–213 (1980).
8. T. Tsuji, *Ann. Rev. Astron. Astrophys.* **24,** 89–125 (1986).
9. R. S. Ram, J. Liévin, and P. F. Bernath, *J. Chem. Phys.* **109,** 6329–6337 (1998).
10. R. S. Ram, J. Liévin, and P. F. Bernath, *J. Mol. Spectrosc.* **197,** 133–146 (1999).
11. R. S. Ram, J. Liévin, and P. F. Bernath, *J. Chem. Phys.* **111,** 3449–3465 (1999).
12. I. Shim, K. Mandix, and K. A. Gingerich, *J. Mol. Struct. (Theochem)* **393,** 127–139 (1997).
13. B. Simard, C. Masoni, and P. A. Hackett, *J. Mol. Spectrosc.* **136,** 44–55 (1989).
14. W. J. Balfour, A. J. Merer, H. Niki, B. Simard, and P. A. Hackett, *J. Chem. Phys.* **99,** 3288–3303 (1993).
15. T. M. Dunn and K. M. Rao, *Nature* **222,** 266 (1969).
16. J.-L. Féménias, C. Athénour, and T. M. Dunn, *J. Chem. Phys.* **63,** 2861–2868 (1975).
17. Y. Azuma, J. A. Barry, M. P. J. Lyne, A. J. Merer, J. O. Schröder, and J.-L. Féménias, *J. Chem. Phys.* **91,** 1–12 (1989).
18. Y. Azuma, G. Huang, M. P. J. Lyne, A. J. Merer, and V. I. Srdanov, *J. Chem. Phys.* **100,** 4133–4155 (1994).
19. T. M. Dunn, private communication.
20. A. Bérces, S. A. Mitchell, and M. Z. Zgierski, *J. Phys. Chem.* **102,** 6340–6347 (1998).
21. H. Sellers, *J. Phys. Chem.* **94,** 1338–1343 (1990).
22. D. A. Fletcher, D. Dai, T. C. Steimle, and K. Balasubramanian, *J. Chem. Phys.* **99,** 9324–9325 (1993).
23. S. R. Langhoff and W. Bauschlicher, Jr., *J. Mol. Spectrosc.* **143,** 169–179 (1990).
24. O. Launila, B. Schimmelpfennig, H. Fagerli, O. Gropen, A. G. Taklif, and U. Wahlgren, *J. Mol. Spectrosc.* **186,** 131–143.
25. B. A. Palmer and R. Engleman, "Atlas of the Thorium Spectrum," Los Alamos National Laboratory, Los Alamos, 1983.
26. G. Huang, Ph.D. thesis, University of British Columbia, Canada, 1993.